doi:10.14311/ppt.2023.3.119
Plasma Physics and Technology **10**(3):119–122, 2023

MULTIPHYSICAL SIMULATION OF IMPULSE CURRENT ARCS IN SPARK GAPS FOR INDUSTRIAL APPLICATIONS

O. Schneider[a,*], D. Gonzalez[b], A. Ehrhardt[a]

[a] *DEHN SE, Hans-Dehn-Strasse 1, 92318 Neumarkt, Germany*

[b] *Leibniz Institute for Plasma Science and Technology, Felix-Hausdorff-Strasse 2, 17489 Greifswald, Germany*

[*] olga.schneider@dehn.de

Abstract. Digital prototyping enables cost-effective production and modular optimization of surge protection devices (SPD). Numerical model of SPD prototypes involves complex multiphysics phenomena. However, the processes related to impulse current arcs in spark gaps are not well understood so far. Limited knowledge exists regarding hydrodynamic effects, plasma states, and radiation properties. This work studies an impulse current 8/20 µs with an amplitude of about 5 kA in experiment and simulation.

Keywords: arc simulation, spark gap, impulse current, surge protection device, radiation heat transfer, magnetohydrodynamics.

1. Introduction

SPD digital prototyping reduces physical testing and shortens product development cycles [1]. The SPD studied in this paper is based on spark gap technology and protects against lightning and overvoltage. The function of spark gap lightning current arresters is to generate an arc discharge and ionize the separation gap. The impulse current is followed by the mains current, which is controlled by the mains voltage. Spark gaps with quenching or deionization chambers have a high capacity to quench follow currents and limit follow currents for both AC and DC. Modern lightning protection systems must safely extinguish short-circuit currents, prevent the release of hazardous gases, and save space. Optimization of geometrical, electrodynamic, gas dynamic, and physical properties is crucial for SPD product development. The multiphysical virtual spark gap tool for SPD digital prototyping presented in [1] was applied for short-circuit current and the processes of arc movement on the electrodes and arc splitting on the splitting plates are shown and compared to experiment. This study examines 8/20 µs impulse current with an amplitude of about 5 kA through both experiments and simulations.

In the lightning, there are two standard pulse waveforms: 8/20 µs and 10/350 µs. 8/20 impulse currents are characterized by the current amplitude increasing from 10% to 90% within 8 µs and decreasing to 50% of the amplitude value in the next 20 µs. 10/350 pulses have a current rise time of 10 µs and a maximum amplitude of about 25 kA for the selected SPD (Figure 1). To enhance the design and performance of SPDs, a better understanding of impulse currents in spark gaps is required. Some studies were done on lightning protection for high-voltage overhead lines. These include simulations of impulse current arc discharges and designing a discharge chamber. One study, e.g. in [2], used a magnetohydrodynamic (MHD) model with local thermodynamic equilibrium (LTE) to investigate a impulse current of 8/50 µs with about 12 kA. The results showed high hydrodynamical processes, such as the high-temperature plasma reaching the chamber outlet at about 15 µs with rod electrodes. The high-pressure zone reaches the discharge chamber outlet due to the compression of cold gas before the high-temperature zone. Another study [3] proposed non-equilibrium plasma processes and used a two-temperature model for impulse current arc discharges in mountainous areas. Results have shown that the arrester's breaking capacity decreases at low ambient pressures.

This paper presents models of an impulse current arc motion along diverging electrodes using FlowVision [4] and the integrated MHD approach [1]. The arc behaviour in an air plasma is described in the LTE state, with plasma properties depending on temperature and pressure. Ablation processes are not considered in this paper. Due to high temperatures, plasma radiation must be taken into account. In [5], low-voltage protective devices were modelled in 2D and 3D axial symmetry using the net emission coefficient (NEC) method. The NEC assumes an infinitely long, isothermal, cylindrical plasma column, and the column's radiative energy loss depends, among other things, on the choice of effective emission radius [6]. This can be difficult to use with an irregularly shaped dynamic arc and with large pressure fluctuations over the column radius according to [6] and [7]. This paper shows use of the discrete ordinate method (DOM) in a spectral approximation involving pressure dependence.

1.1. Experiment and numerical setup

A spark gap with optical access (Figure 1) is used for the impulse current arc investigations; further description of the performed experiments and image recordings of the impulse current arc are available

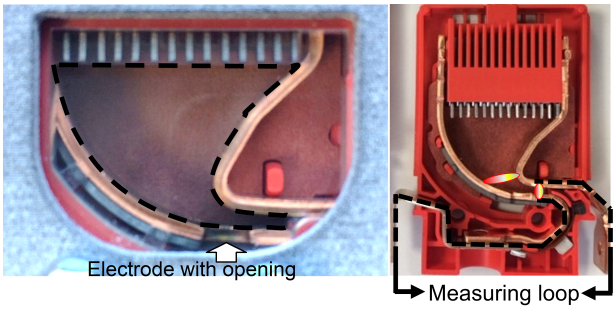

Figure 1. SPD with optical access for video recording and the internal structure of the spark gap.

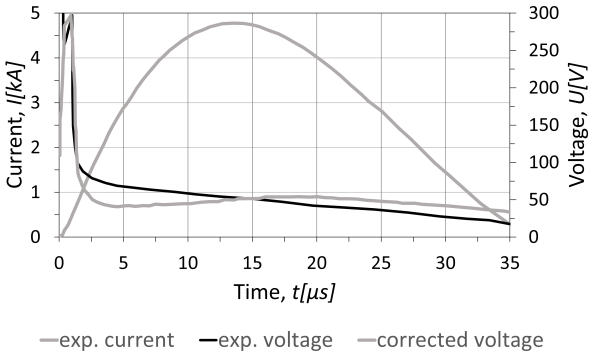

Figure 2. Measured current, voltage and corrected voltage without the inductance of the measuring circuit.

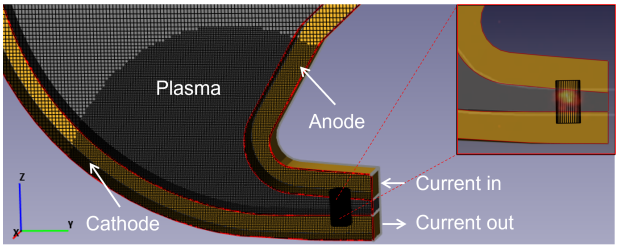

Figure 3. Simplified model for simulation and arc initialization at 1 µs as cylindrical shape with radius ∼0.57 mm and length ∼1.03 mm.

in [8]. The tested unit contains copper electrodes, a deionization chamber, a side wall with vulcanised fibres and a transparent polycarbonate wall. The recorded spectra in [8] show not representative species of carbon and copper in the plasma. Therefore, pure air plasma properties can be applied for the MHD modelling in this work.

Experimental data from recorded arc current and voltage curves (Figure 2) are used to validate simulation results. Especially in the case of transient impulse currents with an impressed current character, the arc voltage provides important information for the verification of the numerical results. Therefore, the measurement of the voltage shall be as accurate as possible. Due to the highly transient change of the current, coupled induced voltages are expected, which lead to over or under estimation of the real arc voltage. By determining the wiring's parasitic inductivity, it is possible to calculate the deviation of the real voltage value caused by coupled inductive effects and to subtract out their amount from the measured voltage. To reduce the parasitic inductivity of the experimental setup, a BNC-connector is used to connect the voltage Probe (LeCroy PPK5000) reducing the length of the measurement wiring to a minimum. In addition, the total length of the current path from the connection bolts along the running rails (the same ones used for the measurement wiring) is determined to find the inductance of the measurement circuit, which was determined to 33 nH. Furthermore, the increase in wiring length caused by the displacement of the arc along the runners is considered. This value was approximated to 1 nH/mm displacement. To determine the timely displacement of the arc during the impulse current the images of a frame camera Specialized Imaging (SIM) with exposure times of 5 ns were used. The real arc voltage can be then approximated as follows $U_{\mathrm{arc}}(t) = U(t) - L_{\mathrm{measuring\ loop}}(t)\mathrm{d}i(t)/\mathrm{d}t$, where the measuring circuit inductance in time is $L_{\mathrm{measuring\ loop}}(t) = 33\,[\mathrm{nH}] + 1\,[\mathrm{nH/mm}]$*arc displacement$(t)\,[\mathrm{mm}]$. An example of the discrepancy between measured and corrected arc voltage is shown in Figure 2.

For the case of only an impulse loading, without main currents, the splitting plates can be excluded from the numerical model. In Figure 1, the modelling area is represented by the black dotted line on the left. The corrected voltage is used for validation of numerical results. Therefore, the simulation model is simplified and includes two electrodes and plasma region, see Figure 3. The cathode has no gas circulation opening like the original unit. The experimental current profile is used for numerical simulation and arc initialization is based on experimental data. The arc ignites between the electrodes after about 1 µs at an arc voltage of about 50 V and a current of about 500 A. The thermodynamic and electrodynamic energies are compared, the electrodynamic energy is about 0.025 J. For the thermodynamic energy, an isochoric process at constant volume is assumed. The arc geometry in the ignition region is determined from image taken at 1 µs. The thermodynamic energy corresponds to a temperature of about 28,000 K. The conversion of electrical energy into kinetic energy up to 1 µs is realised with the volume heat source model [4].

The material data for air plasma and copper electrodes are taken from sources [9] and [10]. The DOM is used with 8 directions to speed up the modelling. The mean absorption coefficients are taken from various sources and four radiation cases are studied in detail, see Table 1. The mean absorption coefficients of the nitrogen plasma are also examined here, since according to [11] the radiation properties of air are very similar to pure nitrogen plasma. In this work, the mean absorption coefficients are extended for pressure dependence by multiplying them by a factor (absolute pressure divided by reference pressure) based on the relationship between pressure and absorption coeffi-

Case	Plasma data description	Source
(a)	without radiation	-
(b)	nitrogen with 6 bands	[7]
(c)	air with 10 bands	[13]
(d)	air with 12 bands - Planck mean	[14]

Table 1. Four radiation cases for simulations.

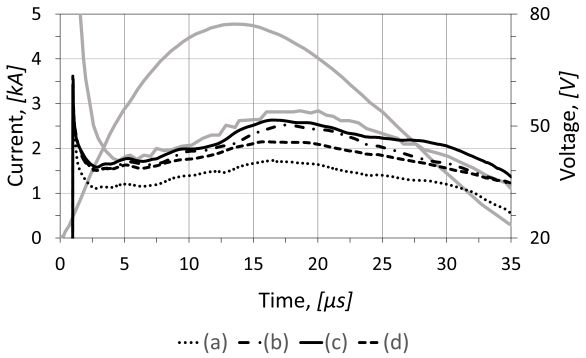

Figure 4. Comparison of the corrected voltage (grey line) from Figure 2 with the calculated voltages for cases shown in Table 1.

cient shown in [12]. It is assumed that the device has been used several times for experiments. Therefore, the emission values for the copper electrodes, vulcanised fibre wall and transparent wall are assumed to be 0.8, 0.95 and 0.3 respectively. The temperature of the outer walls is set to 300 K. The conjugate boundary condition is between the electrodes and the plasma. The voltage drop for copper electrodes in air is assumed to be 16.5 V [12] and the arc root model with current density-voltage characteristics at the gas-solid interfaces is used [1].

2. Results

Figure 4 shows the comparison of the numerical voltage profiles with corrected voltage from the experiment. All numerical voltage shapes have a similar shape compared to the experimental voltage profile: the voltage rises to 18 µs and then falls. The curves (c) with air plasma data and (b) with nitrogen data show similar voltage values and are closer to the experimental voltage values. The maximum temperature values (see Figure 5) with the nitrogen plasma data are allocated in the region of 30,000K and slightly higher compared to the air plasma data from [13], so that the simulation results agree with the statement from [11]. The simulation without radiation process (case (a) in Table 1) shows the highest temperature in Figure 5 and the lowest voltage in Figure 4. This is because the plasma radiation dominates the heat transfer. The case (d) uses values of Planck mean absorption coefficients for 12 frequency groups with non-uniform splitting. In [14] it is suggested to use it when the system is absorption dominated. In this case,

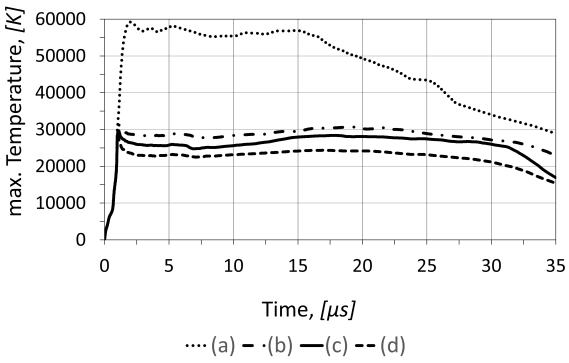

Figure 5. Comparison of calculated temperatures for cases shown in Table 1.

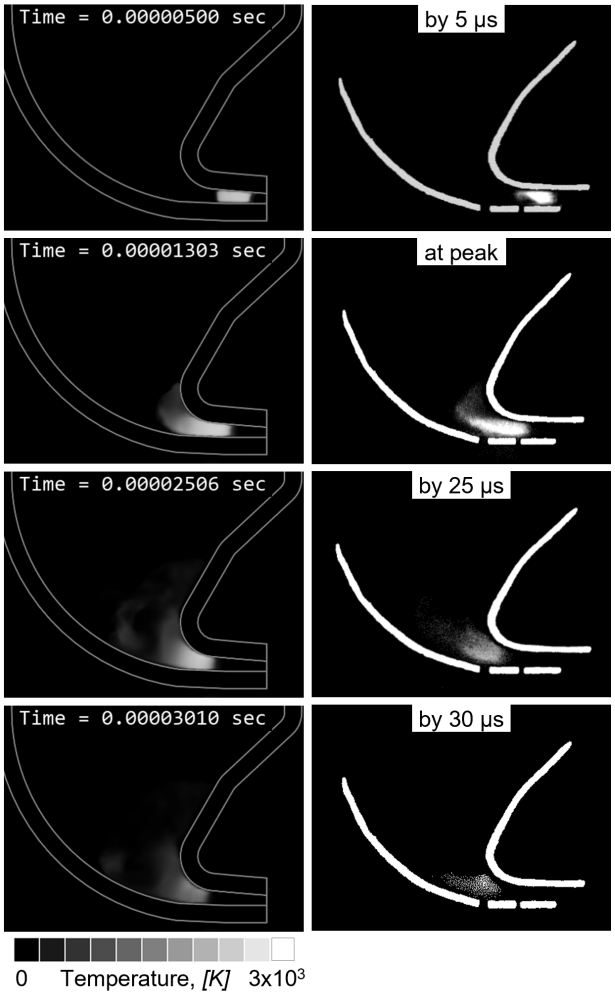

Figure 6. Left side: simulated arc shapes (highest temperature of all cutting planes) for case (c). Right side: framing camera images with light intensity (framing camera SIMD8, CCD sensor, 12 bit resolution, 5 ns exposure time) [8].

the lowest temperature is observed, which is in the range of 17,000–25,000 K. At the same time, the voltage profile of case (d) has a lower voltage maximum at 18 µs.

The simulated arc shapes (left side of Figure 6) of case (c) in Table 1 using air plasma data from the

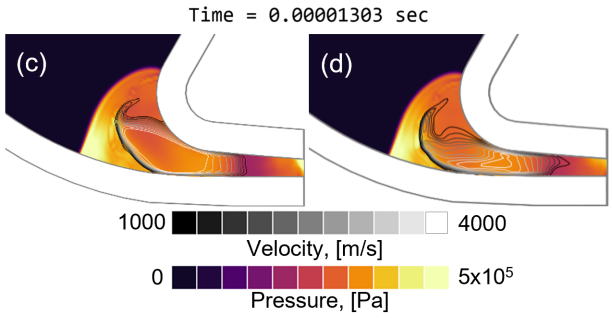

Figure 7. Comparison of pressure distribution in cases (c) and (d) and contour plot of velocity distribution (isotaches) in the arc column for both cases.

reference [13] closely match the shapes and temporal positions observed in the high-speed images in [8] (right side of Figure 6). These results were achieved using a fine mesh size of about 0.1 mm, as shown in Figure 3. The plasma area has high velocities with a Mach number reaching about 1.5. The combination of fine mesh and high velocities leads to very small time steps in the range of 10^{-8}–10^{-9} s.

Figure 7 shows the comparison of numerical results with air plasma data in cases (c) and (d) at a current peak time of about 13 µs. In case c, the isotaches are denser, showing a higher velocity gradient. The pressure wave in case (c) is faster compared to case (d). The pressure distribution in the arc plasma is not uniform in both cases and lies in the range of about 3–3.5 bar. The arc plasma velocity in case (c) is higher than in case (d), causing deformation and producing the voltage and arc shape corresponding to the experiment. In case (d), high absorption coefficient values strongly absorb energy, reducing temperature and arc plasma velocity. However, according to the voltage result in case (d), the absorption is too high, as mentioned in [14].

3. Conclusions

The simulation results of the simplified model for the waveform 8/20 µs with a current amplitude of about 5 kA in case (c) are in good agreement with the experimental data. For larger impulse currents, a finer grid is required to accurately represent the flow velocity, which affects the arc shape, position, and voltage in the device. The plasma radiation data also has a significant impact on the hydrodynamic processes in the arc plasma. The arc ignition plays an important role in modelling the initial arc energy. The high-speed camera images helped to determine the start of the arc. The numerical pressure agrees well with the experimental work in [8], but the numerical arc temperature is higher. Further investigation should be carried out using a more complex simulation geometry with gas circulation corresponding to the experimental design. Additionally, a non-LTE model could be considered during the ignition and current rise phase, as suggested in [8].

References

[1] O. Schneider, A. Ehrhardt, B. Leibig, et al. Surge protection device digital prototyping. In *30th International Conference on Electrical Contacts*, pages 486–493, Switzerland, 06 2021.

[2] I. Murashov, V. Frolov, D. Uhrlandt, et al. Analysis of arc processes in multi-chamber arrester for lightning protection at high-voltage overhead power lines. *Plasma Physics and Technology Journal*, 4(2):124–128, 2017.

[3] V. Frolov, D. Ivanov, A. Sivaev, and A. Chusov. Development of two-temperature mathematical model of processes in discharge chamber of multi-chamber arrester operating in conditions of mountain areas. *Plasma Physics and Technology Journal*, 6(2):135–139, 2019. doi:10.14311/ppt.2019.2.135.

[4] Medividia BV. *FlowVision Software*. https://flowvisioncfd.com/en.

[5] M. Baeva, M. Hannig, R. Methling, et al. Predictive capability and efficiency of 2D planar against 3D models of LV interrupters. In *31th International Conference on Electrical Contacts*, Sapporo, 06 2022.

[6] J. Zhong, F. Yang, W. Wang, et al. Net emission coefficient and radiation transfer characteristics of thermal plasma generated in nitrogen-ptfe vapor mixture. *IEEE Transactions on Plasma Science*, 46(4):990–1002, 2018. doi:10.1109/TPS.2018.2814399.

[7] J. Huo, Y. Wang, and Y. Cao. 3D computational study of arc splitting during power interruption: The influence of metal vapor enhanced radiation on arc dynamics. *Journal of Physics D: Applied Physics*, 54, 10 2020. doi:10.1088/1361-6463/abc64b.

[8] M. Baeva, R. Methling, D. Gonzalez, et al. Complementary experimental and simulation-based characterization of transient arcs. *Plasma Physics and Technology Journal*, 10(2):56–59, 2023. doi:10.14311/ppt.2023.2.56.

[9] A. D'Angola, G. Colonna, C. Gorse, and M. Capitelli. Thermodynamic and transport properties in equilibrium air plasmas in a wide pressure and temperature range. *European Physical Journal D*, 46(1):129–150, 2008.

[10] A. Mutzke. *Lichtbogen-Simulation unter besonderer Berücksichtigung der Fußpunkte*. PhD thesis, TU-Braunschweig, 2009.

[11] V. Aubrecht and M. Bartlova. Radiation transfer in thermal plasmas of air, N2 and CO24. In *17th International Conference on Gas Discharges and Their Applications*, 2008.

[12] C. Rümpler. *Lichtbogensimulation für Niederspannungsschaltgeräte*. Fraunhofer-Verl., Stuttgart, 2009.

[13] R. Fuchs. Numerical arc simulations of radiatively-induced pmma nozzle wall ablation. In *30th International Conference on Electrical Contacts*, pages 466–473, Switzerland, 06 2021.

[14] N. Bogatyreva, M. Bartlova, and V. Aubrecht. Mean absorption coefficients of air plasmas. *Journal of Physics: Conference Series*, 275(1):012009, 01 2011. doi:10.1088/1742-6596/275/1/012009.